Magnetic Control of Protein Spatial Patterning to Direct Microtubule Self-Assembly

Céline Hoffmann,[†] Elsa Mazari,[‡] Charlie Gosse,[‡] Louise Bonnemay,[†] Sarah Hostachy,[†] Jérémie Gautier,[†] and Zoher Gueroui[†,*]

[†]Department of Chemistry, Ecole Normale Supérieure, UMR 8640 CNRS-ENS-UPMC Pasteur, 24 rue Lhomond, 75005 Paris, France and [‡]Laboratoire de Photonique et de Nanostructures, LPN-CNRS, route de Nozay, 91460 Marcoussis, France. C.H. and Z.G. conceived and designed the experiments. C.H., L.B., S.H., J.G., and E.M. performed the experiments. All authors analyzed the data. C.H. and Z.G. wrote the manuscript, and all authors commented on it.

ABSTRACT Living systems offer attractive strategies to generate nanoscale structures because of their innate functional properties such as the dynamic assembly of ordered nanometer fibers, the generation of mechanical forces, or the directional transport mediated by molecular motors. The design of hybrid systems, capable of interfacing artificial building blocks with biomolecules, may be a key step toward the rational design of nanoscale devices and materials. Here, we have designed a bottom-up approach to organize cytoskeletal elements in space using the self-assembly properties of magnetic nanoparticles conjugated to signaling proteins involved in microtubule nucleation. We show that magnetic nanoparticles conjugated to signaling proteins involved in microtubule nucleation can control the positioning of microtubule assembly. Under a magnetic field, a self-organized pattern of biofunctionalized nanoparticles is formed and leads to the nucleation of a periodical network of microtubules in *Xenopus laevis* egg extract. Our method shows how bioactive nanoparticles can generate a biochemically active pattern upon magnetic actuation, which triggers the spatial organization of nonequilibrium biological structures.

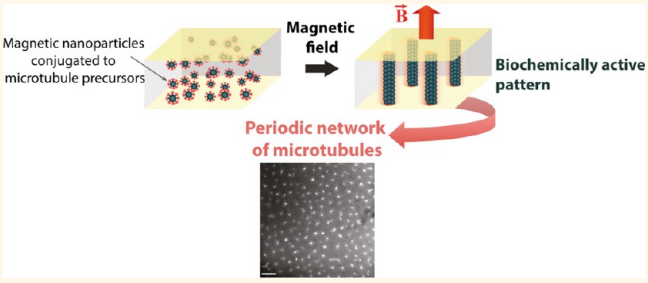

KEYWORDS: self-organization · protein signaling · magnetic nanoparticles · biological materials · self-assembly · microtubule · magnetogenetics

The design of hybrid systems, capable of interfacing artificial building blocks with biomolecules, is a key step toward the rational design of nanoscale devices and materials[1,2] and offers to bridge the gap between top-down and bottom-up approaches.[3,4] Patterning techniques using top-down approaches such as microcontact printing,[5,6] photolithography,[7] and nanoparticle-based protein patterns[8] are powerful tools of control at the molecular, cellular, and tissue scales. Notably, surface patterning of proteins has increased the understanding of numerous processes, from protein–protein interactions,[9] to cell behavior, such as extracellular matrix–cell interactions,[10,11] cell spreading and adhesion,[12] or neurite outgrowth.[13] Complementary to these surface patterning techniques, bottom-up approaches that use the self-assembly properties of interacting species, including macromolecules or colloidal particles, have been used to generate specific patterns and engineer new materials.[14–16] DNA, the cellular membrane, and the cytoskeleton are just several examples of the many self-association processes based on the intrinsic properties of biomolecules found within biological systems.[17–20] The physical properties of cytoskeleton proteins can be exploited to generate new materials having novel properties[21–24] or hybrid assemblies with inorganic nanoparticles.[25,26] Expanding on this domain, microtubule (MT) fibers have unique mechanical and chemical properties that permit efficient directional transport of cargos using specific molecular motors powered by ATP.[27,28] The transport of specific molecular components at the mesoscopic scale could therefore be achieved without requiring mass transport along fluid pressure gradients.[29] In addition, networks of microtubule asters could be used as programmed bioinspired templates with perspectives including the

* Address correspondence to zoher.gueroui@ens.fr.

Received for review May 6, 2013 and accepted October 15, 2013.

Published online October 16, 2013
10.1021/nn4022873

control of the positioning or growth of inorganic materials[26] and functional devices such as optical devices.[30]

The assembly of magnetic colloidal particles under magnetic field has allowed for the generation of various spatial structures, such as linear arrays[31,32] and ring colloidal superstructures.[33] For instance, linear arrays of particles have been used as templates for examining the mitotic spindle morphogenetic properties or as force sensors during actin filament polymerization.[34,35] Magnetic nanoparticles conjugated to proteins were used to trigger specific signaling pathways involved in cellular functions.[36−41] Moreover, magnetic beads that were self-assembled into a quasi-regular array of columns have been successfully used in a broad range of applications, including DNA separation,[42,43] protein digestion,[44] and cell sorting.[45] Here, we demonstrate a bottom-up approach to organize cytoskeletal elements in space using the self-assembly properties of magnetic nanoparticles. We show that magnetic nanoparticles conjugated to signaling proteins involved in microtubule nucleation can dictate the positioning of microtubule assembly. Under magnetic field, a self-organized pattern of biofunctionalized nanoparticles is formed and leads to the nucleation of a periodical network of MTs in *Xenopus laevis* egg extract. Our method shows how bioactive nanoparticles can generate a biochemically active pattern upon magnetic actuation that triggers the spatial organization of nonequilibrium biological structures.

RESULTS AND DISCUSSION

In order to generate a spatial biochemically active pattern, we designed an assay allowing for the control of the periodic nucleation of microtubule fibers using self-assembled magnetic nanoparticle arrays. Iron oxide nanoparticles (120 nm) were conjugated to a promoting factor of MT polymerization, RanGTP.[40] We first examined the conjugation of purified RanGTP to carboxylic-functionalized magnetic nanoparticles (Ran−NPs) through their biofunctionality and their ability to induce MT assembly (Figure 1 and see Experimental Section). Variation of the initial RanGTP:NP reactant ratio allowed us to tune the amount of protein−nanoparticle conjugation (Figure 1b). We found that almost 70% of the protein initially bound to nanoparticles remained conjugated after several hours (Supporting Information Figure S1).

In reconstituted functional cytoplasm, microtubule nucleation has been previously described as highly sensitive to RanGTP concentration with a nucleation threshold of about 3 μM.[40,46] During microtubule growth, dynein molecular motors assembled the fibers into very stereotyped radial arrays called asters.[47,48] We monitored aster assembly as a function of increasing concentration of Ran−NP complexes ([RanGTP] = 1 to 6 μM for Ran:NP between 700 and 1000) and compared the results to data with uncoupled RanGTP. We found that microtubule polymerization follows a sigmoidal response with RanGTP concentration under both conditions (proteins coupled to NPs or uncoupled proteins) as previously described (Figure 1c).[40] Both RanGTP conjugated to NPs and uncoupled RanGTP promote MT nucleation with a switch-like behavior with concentration threshold of about 4 μM.

We used the biochemical sensitivity of the MTs to remotely control the aster formation using self-assembled magnetic nanoparticle arrays (Figure 2a). In principle, the accumulation of nanoparticles conjugated to RanGTP (Ran−NP) as columns will induce a strong local increase of RanGTP concentration exceeding the concentration threshold and will locally trigger microtubule nucleation (Figure 2a).

The NP concentration and magnetic field strength were tuned to promote robust column formation within cell extracts. *Xenopus* egg extract containing NPs was placed in a PDMS microfluidic channel (45 μm height × 1 mm large, see Experimental Section). A magnetic field perpendicular to the channel was applied during 10 min at 65 mT, which was strong enough to induce the aggregation of the magnetic nanoparticles into columns. Then the magnetic field was decreased to 25 mT during the experiment course to avoid a temperature increase due to Joule dissipation in the electric coil. The magnetic field

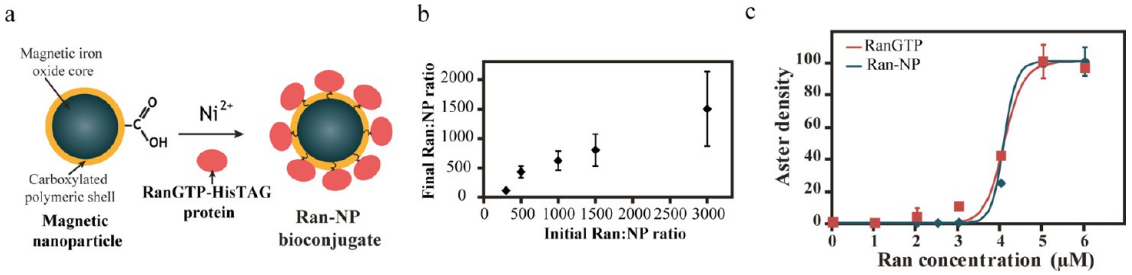

Figure 1. Synthesis and characterization of Ran−NP complex. (a) Ran is conjugated to magnetic nanoparticles by chelation of nickel ions between the carboxylic acid function presented at the nanoparticle surface and the polyhistidine tag of RanGTP recombinant protein. (b) Control of conjugation stoichiometry. By varying the initial ratio of Ran per nanoparticle, the number of Ran conjugated per nanoparticle can vary between 100 to 1500. (c) Microtubule nucleation and aster assembly are ultrasensitive to the concentration of RanGTP (red line) or Ran−NPs (green line). Aster density was determined by fluorescence microscopy and normalized to reach 100% for the plateau at the highest RanGTP concentration.

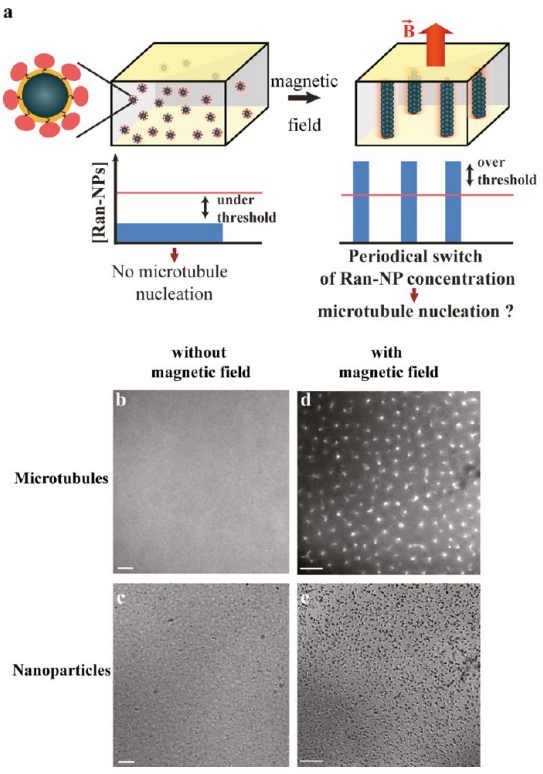

Figure 2. Formation of an array of Ran−NP columns using magnetic field trigger microtubule assembly in a switch-like behavior. (a) Principle of a periodical magnetic switch of Ran−NP concentration. Magnetic nanoparticles conjugated to RanGTP were placed into a microfluidic channel at a concentration below the MT nucleation threshold. The application of an external magnetic field leads to the formation of magnetic columns parallel to the field. At the vicinity of the Ran−NP columns, the concentration of Ran is larger than the nucleation threshold. (b−e) *Xenopus* egg extract containing Ran−NPs ([Ran] = 1.5 μM, [NP] = 2 nM), and fluorescent tubulin (100 nM) was placed in a microfluidic channel in absence (b,c) or presence (d,e) of a magnetic field (65 mT). (b,d) Observation by fluorescence microscopy of microtubule assemblies. (c,e) Microscopic observation of nanoparticles under brightfield illumination. Bar = 50 μm.

induced the alignment of the magnetic moment of each nanoparticle along the field and promoted their local attraction through dipole−dipole interactions. This process led to formation of nanoparticle columns regularly spaced (Supporting Information Figure S2). We found that a minimum of 0.5 nM of NPs allow the self-assembly of an array of columns with an interdistance of about 7.5 μm within 10 s in egg extracts (Supporting Information Figure S3). In addition, the spacing between columns does not vary with the nanoparticle concentration (Supporting Information Figure S3), in agreement with previous observations.[49] Closer look to the column diameter shows that the structures are made of several chains of nanoparticle aggregates (Supporting Information Figure S4). This effect can be explained by the formation of a protein corona around the nanoparticles within the egg extract that may promote nonspecific aggregation of the nanoparticles (see Supporting Information).[50]

Next, we investigated the effect of Ran−NP column assembly on MT nucleation. Ran−NPs were added at an initial concentration such that the relative concentration of bound RanGTP was under the MT nucleation threshold in egg extract ([Ran] = 1.5 μM and [NPs] = 2 nM). Microtubule fibers were detected by supplementing the extracts with 100 nM of fluorescently labeled tubulin (see Experimental Section).[51] Without magnetic field, *e.g.*, in absence of column formation, and with a Ran−NP concentration of 1.5 μM, no MT nucleation was observed (Figure 2b,c). In contrast, at the same Ran−NP concentration, upon magnetic field, *e.g.*, in presence of an array of Ran−NP columns (Figure 2e), we observed the formation of fluorescent MT bundles organized in radial asters with a distinguished pole (Figure 2d). MTs could be observed 20 min after application of magnetic field as thin fibers that continued to evolve until they formed arrays of MTs organized in asters, after 35 to 40 min (Supporting Information Figure S5). The time scale of MT assembly was similar to experiments performed with uncoupled RanGTP proteins, consistent with the microtubule polymerization rate in extracts, which is 0.5−2 μm min^{-1}. Using confocal microscopy, we found that the asters were localized a few micrometers above the coverslide of the microfluidic channel with a thickness of about 4 μm (Supporting Information Figure S6). Therefore upon magnetic field application, the localization of RanGTP at the surface of the columns was sufficient to trigger MT polymerization. We estimated that our system allows a local enhancement of the concentration of 40 fold the initial Ran concentration (see Experimental Section). Next, we quantified the structure of the microtubule patterns. From quantification by autocorrelation analysis ($N = 4$), we found that asters were positioned periodically with an interdistance periodicity of 30 ± 6 μm (Figure 3a,b) while the nanoparticle interdistance was 7.5 ± 2.1 μm (Figure 3e−h). In addition, using fast Fourier transform analysis, we found that the MT networks were organized as a hexagonal phase (Figure 3c,d). We then investigated the conditions required to obtain a periodic network by varying the stoichiometry of Ran per nanoparticle and the initial concentrations of RanGTP and NP (Figure 4). We found that a minimum of 550 Ran per NP was necessary to induce MT nucleation and that a RanGTP concentration ranging from 1 to 3.5 μM generated a periodic MT network. Above 3.5 μM, a disordered network of MTs was observed (Figure 4). Altogether these observations demonstrate that the formation of Ran−NP columns upon magnetic stimulation leads to a robust biochemical switch triggering the assembly of a regular array of microtubule fibers.

Microtubule assembly using freely diffusing (unbound) RanGTP was monitored to investigate the role of the magnetic nanoparticles in generating periodic structures. In the presence of free RanGTP (1.5 μM, in egg

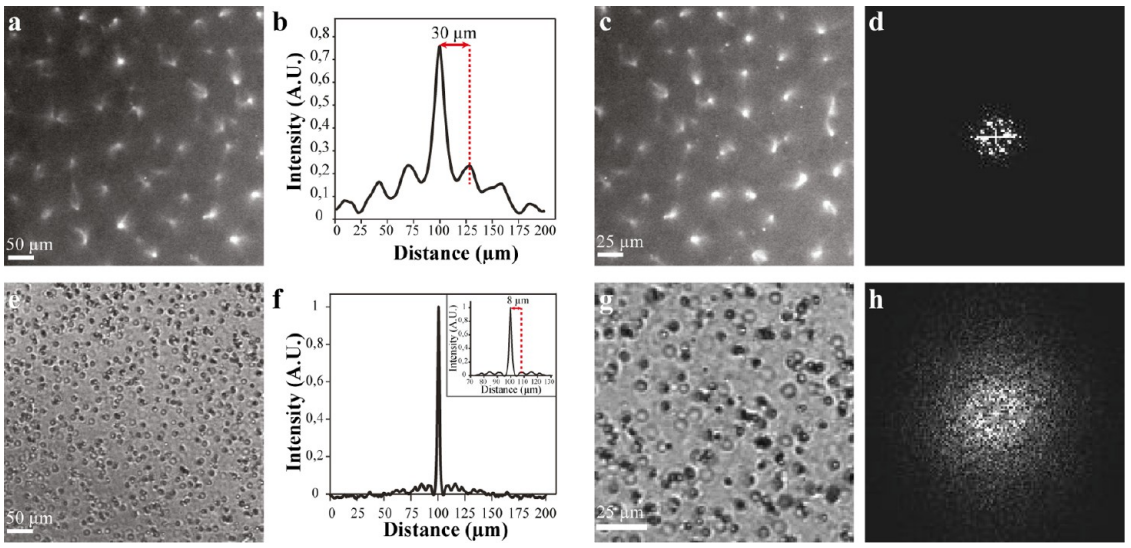

Figure 3. Periodical switch of RanGTP concentration generates a periodical network of microtubules. *Xenopus* egg extract containing Ran−NPs ([Ran] = 1.5 μM, [NP] = 2 nM) and fluorescent tubulin (100 nM) was placed in a microfluidic channel in presence of magnetic field. (a,c) Observation by fluorescence microscopy of microtubule assemblies. (e,g) Microscopic observation of nanoparticle arrays under brightfield illumination. (b,f) Autocorrelation profile for microtubules (b) and Ran−NP patterns (f). They give an average distance between microtubule asters of 30 μm (b) or between Ran−NP columns of 8 μm (f). Fourier transform analysis of microtubule structures (d) and nanoparticle column arrays (h) obtained under magnetic field.

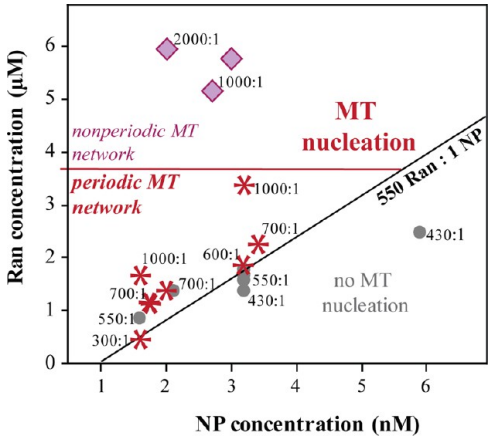

Figure 4. Effect of NP and Ran concentration on microtubule patterns under magnetic field. This phase diagram shows that a minimum of 550:1 Ran per NP is necessary to induce microtubule nucleation. RanGTP initial concentration should range from 1 to 3.5 μM to observe a periodic network. (Number of independent experiments = 20).

extract and within the microfluidic channel), no microtubule nucleation was observed regardless of magnetic field application (Figure 5a,b). Above the nucleation threshold (RanGTP = 6 μM), we observed the assembly of asters (Figure 5c,d). Interestingly in this later case, MTs were first organized into a connected network of fibers that start to collectively collapse after 10 min all over the channel and over hundreds of micrometers until reaching a steady state with structures of 200 μm width.

Then, to clarify the role of the spatial distribution of RanGTP concentration in determining the periodical organization of MT asters (Figure 2), we next investigated the influence of the magnetic column matrix by comparing MT nucleation in presence of RanGTP and unconjugated nanoparticles or in presence of Ran−NPs. In the presence of RanGTP and unconjugated nanoparticles, we observed an absence of MT nucleation at 1.5 μM as expected (Figure 5e,f), whereas at 6 μM, microtubule assemblies formed isolated and contracted bundle-like structures that did not collapse as much as in experiments performed in the absence of nanoparticles (Figure 5g,h) The morphology of the MT networks in those conditions is independent of the magnetic field strength. When the Ran−NP complexes (1.5 μM) were added in the solution but without a magnetic field, no MT nucleation was observed (Figure 5i). This is in contrast with experiments performed in presence of magnetic columns (Figure 5j). In the presence of Ran−NPs at a concentration of 6 μM, we observed that MT assemblies were similar (Figure 5k,l) to those found in the conditions of unbound RanGTP (Figure 5g,h). In addition these organizations did not present any periodical organization as shown by Fourier transform analysis (Supporting Information Figure S7).

Therefore, the spatial organization of microtubule patterns depends drastically on the presence of nanoparticles. More precisely, the large-scale contraction is not observed in presence of NPs for every cases: NPs conjugated or not to Ran and NPs forming columns or not.

To investigate the mechanism driving the aster fusion process, we next examined the role of dynein motors. In presence of an inhibitor of dynein ATPase activity, Na-orthovanadate, MTs formed isolated fibers, randomly orientated and homogeneously distributed over the entire length of the microchannels (Supporting Information Figure S8). This result shows

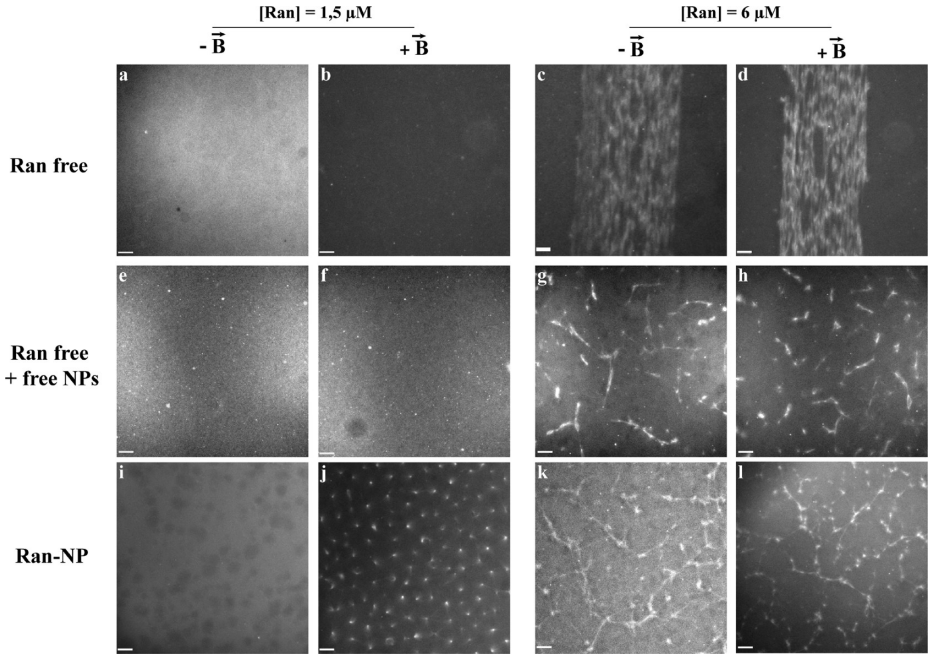

Figure 5. Comparison of microtubule network organization under different conditions: RanGTP concentration, presence of magnetic field, conjugated or unconjugated nanoparticles. *Xenopus* cell extract supplemented with 100 nM fluorescent tubulin and containing RanGTP, RanGTP and free nanoparticle, or Ran−NP at the indicated concentration (1.5 or 6 μM) was placed in microfluidic channel. Microtubule network formation was observed under application of magnetic field (+B) or not (−B). Bars: 25 μm.

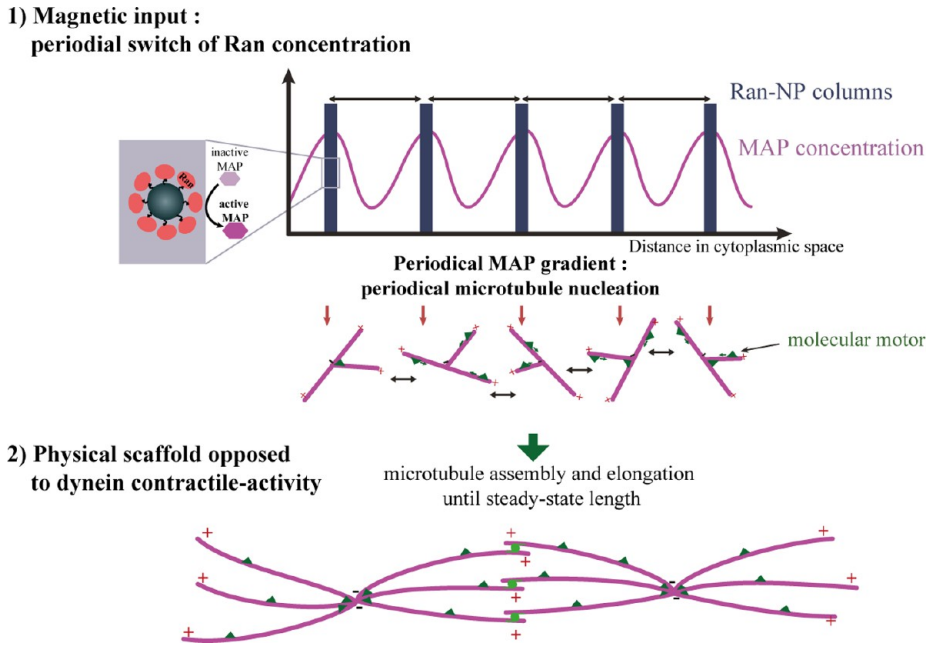

Figure 6. Periodical network of microtubules is generated both by periodical concentration of Ran proteins and by molecular motors. Schematic of the generation of aster networks induced by Ran−NP columns. First, under magnetic field, Ran−NP self-organized into periodical columns. This periodical accumulation of Ran activates the microtubule nucleators (MAPs) at the vicinity of the columns, leading to the nucleation of microtubule in a restricted space. Second, the interplay between molecular motors and growing microtubules leads to the formation of an aster network, and presence of magnetic nanoparticle scaffold limits the contractility of microtubules, leading to the organization of the final periodical aster network.

the essential role of dyneins in generating large-scale reorganization of the network through a contraction-fusion process.

The presence of nanoparticles in the extract resulted in a decreased spatial extension of the MT network contraction−fusion process. However, our results also showed that the patterning of unconjugated nanoparticles was not sufficient to achieve a periodical positioning of MT asters. Taken together, a combination of a physical matrix of nanoparticle columns

and a periodical concentration in space of Ran protein is key to trigger microtubule periodical organization.

By using magnetic nanoparticles conjugated to RanGTP, we showed that we could generate a robust biochemical switch triggering MT nucleation that leads to a periodical organization of aster network. Several elements can explain the steady state aster network formation. The positioning of Ran–NP columns induces the spatially restricted activation of MT nucleators (microtubule associated proteins, MAPs) that trigger the nucleation of the fibers (Figure 6), in agreement with studies showing that a point source of RanGTP coupled to NPs generates localized MT polymerization through reaction diffusion processes.[40] Dynein motor activity will favor the fusion and coalescence of nascent MT-based structures.[52] Indeed, during the MT assembly process, the fibers are first organized in bundles and then in asters by dynein motors, which cross-link, sort, and promote fiber sliding and translation (Supporting Information Figure S5). The MT steady state length is about 15 μm in meiotic *Xenopus* egg extracts and determines the 30 μm-aster diameter. Finally, the array of magnetic columns limits the contractility of MT aster network by providing a physical scaffold opposed to dynein motor activity. Therefore, two coupled mechanisms may be involved in generating the periodical organization of MT networks. First, the periodical distribution of Ran–NPs induces a localized nucleation of microtubules. Second, growing MT fibers at restricted sites are organized by molecular motors until reaching a periodic aster network with a typical length scale set by the microtubule dimension (Figure 6).

CONCLUSIONS

Our results demonstrate that the patterning of signaling proteins allows for the spatial control of MT nucleation and organization. The interplay between the spatial patterning of microtubule nucleators and the self-organizing properties of the fibers under motor activity leads to the formation of a periodic hexagonal network of asters. Our system provides a bottom-up approach of biochemical patterning using magnetic control of signaling protein spatial organization. Further strategies based on the process of nanoparticle assembly or on the mechanism of cytoskeleton assembly may increase the spatial control of cytoskeleton pattern formation. For instance, tuning physical parameters such as the confinement height of the microfluidic channel, the ability of localizing the magnetic field by using an array of nickel dots, or changing the NP interactions through their size and composition can offer relevant future opportunities. On the other hand, biological systems offer a large protein toolbox that could be used to enlarge the possibility of molecular controls at works. The aster diameter could be tuned by adding either specific MAPs that change the fiber lengths in extracts, such as XMAP215,[53] or cyclin dependent kinase proteins.[54] For instance, similar studies could be extended to other biopolymers involved in cell architecture. As an example, the spatial control of actin nucleators may generate additional cytoskeleton organizations with various topologies such as dendritic networks or parallel bundles.[55,56] In addition, our method could be used as a framework for achieving molecular transport[57] and generating new bioinspired materials.[30,58,59]

EXPERIMENTAL SECTION

Reagents. ATP, DDT, creatine phosphate, creatine phosphokinase, mineral oil (M5904), Na-orthovanadate were purchased from Sigma-Aldrich (St Louis, MO). Tubulins, labeled with X-Rhodamin or with FITC, were ordered from Cytoskeleton, Inc. (Denver, CO). All the experiments were done in metaphase extracts. RTV 615 PDMS was from Momentive (Columbus, OH) and SU8-2050 from Microchem (Newton, MA). Cytostatic-factor-arrested (CSF) *Xenopus laevis* egg extracts, which correspond to "active" cytoplasm of oocytes arrested in metaphase II of meiosis, were prepared as previously described.[60]

Expression and Purification of Recombinant Proteins. Expression of plasmid and purification of recombinant proteins were realized as previously described.[61] The plasmids for *Escherichia coli* expression of RanQ69L-GTP (pQE32-Ran, 6His Tag) were kindly provided by Iain Mattaj (EMBL).

Microtubule Nucleation in *Xenopus laevis* Egg Extracts. Microtubule structures were assembled in metaphase *Xenopus* egg extracts containing X-Rhodamin-labeled tubulin (200 nM final), an ATP regenerating system (1 mM ATP, 10 mM creatine phosphate, 100 μg/μL of creatine phosphokinase, final concentrations) and DTT (2 mM final). This mixture was then incubated in the presence of protein and/or magnetic particles at the final concentration indicated in the manuscript. All the experiments were performed in a temperature-controlled room at 18 °C.

Magnetic Nanoparticles. *Conjugation of Protein to Magnetic Nanoparticles.* Superparamagnetic nanoparticles (120 nm diameter, Carboxyl Adembeads 0211, Ademtech, Pessac) were made of a Fe_2O_3 magnetic core encapsulated by a highly cross-linked hydrophilic polymer shell. Their surface displays a carboxylic acid functionality. The initial concentration in nanoparticles was equal to 78 nM. For conjugation to RanQ69L-GTP, 90×10^{-15} moles of magnetic nanoparticles were placed in XB1 buffer (Hepes 10 mM, $MgCl_2$ 1 mM KCl 100 mM Sucrose 50 mM, pH 7.7) by three successive rinses under magnetic field. Then, $NiCl_2$ (2 mM final) and proteins were added at a concentration corresponding to an initial molar ratio of 1500 protein/NP. After 30 min reaction at 4 °C, unconjugated proteins were purified by 3 rinses in XB1 under magnetic field. After purification, we set the concentration of nanoparticle around 60 nM. Conjugation stoichiometry and stability were determined by a semiquantitative assay using SDS-PAGE electrophoresis.[40]

Pegylation of Nanoparticles. For control experiments, we conjugated a hydrophilic polymer (PLL-PEG, Susos) to the nanoparticles. PLL (20 KDa) grafted with PEG (2 KDa) having Lys units/PEG chains = 3.5. PLL-PEG was added to carboxylated nanoparticles at an initial ratio of 100 PEG/COOH in XB1 buffer overnight at 4 °C. After conjugation, the excess of PLL-PEG was removed by 2 successive rinses on permanent magnet with XB1 (wash volume = conjugation volume).

Microfluidic Devices. Master templates were first fabricated on silicon wafers using the SU8-2050 negative photoresist and

PDMS stamps were obtained by conventional replica molding. After unmolding, the elastomeric material was washed with ethanol and dried with a nitrogen flux. Microchannels were then sealed with glass cover slides that have been similarly processed. Tight bonding was obtained by baking at 60 °C overnight. Fluidic features were 47 μm high, 1 mm wide, and 3 mm long.

Formation of Nanoparticle Columns under Magnetic Field. Self-organization of Ran−NPs under magnetic field was performed as follows: cell extract, X-rhodamine tubulin, ATP regenerating system, DTT, and Ran−NPs ([Ran] = 1.5 μM and [NPs] = 1.8 nM final) were mixed at 4 °C before injection in microfluidic channel. Channels were sealed with adhesive tape and immediately placed on microscope. Magnetic field was applied using an electromagnet. A magnetic field of 65 mT was first applied during 10 min, and then external field was decreased until 25 mT throughout the remaining time of the experiment. We estimated that each column is composed of an average of 1600 nanoparticles (based on the number of column/volume unit and on the total number of nanoparticles) and occupied a volume of 43 μm^3. Starting from a homogeneous Ran concentration of 1.5 μM and a conjugation stoichiometry of 1000 Ran per nanoparticles, we calculate the number of Ran molecules per column that lead to a local Ran concentration of 60 μM, meaning a 40 fold increase in Ran local concentration around magnetic column.

Imaging and Data Analysis. Fluorescence imaging of microtubules asters was performed using an IX81 (Olympus) microscope and ×10 (PlanN, NA 0.25), ×20 (UPlanFLN, NA 0.5) and ×40 (UPlanFLN, NA 1.30) objectives, equipped with an EM-CCD (C9102, Hamamatsu, Corporation, Sewickley, PA). Microscope settings and functions were controlled using Simple PCI software (Hamamatsu). Image analysis was performed using Image J Software (Scion Image) and Simple PCI software. Brightfield illumination was used to monitor nanoparticle accumulation.

Data Analysis. In order to precisely characterize microtubules networks orientation and spacing, Fourier tranform (FT) computations were achieved relying on the Image J software (Scion). However, when a regular lattice could not be obtained, we analyzed images by computing autocorrelation functions with the DigitalMicrograph software (Gatan). More exactly, the latter tool realizes a FT of the considered image and multiplies it by its complex conjugate before performing the normalized inverse FT. Autocorrelation intensity profiles were finally achieved by angular integration.

Conflict of Interest: The authors declare no competing financial interest.

Acknowledgment. The authors thank I. Mattaj and B. Koch for the RanQ69L expression plasmid. Thanks also go to V. Marchi, R. Le Borgne, and the members of the Biophysical Chemistry Center of ENS for fruitful discussions, X. Zhao for technical assistance with PDMS processing, A. Cattoni for lending us the magnetic coil, and Joe Dragavon of the Plate-Forme d'Imagerie Dynamique, Imagopole, Institut Pasteur, for critical reading of the manuscript. This work was supported by the CNRS (MI Emergence, Peps-PSL), the Association pour la Recherche sur le Cancer (SFI20101201426), the Ligue Nationale Contre le Cancer (LNCC, 2009), Ville de Paris "Emergence(s)" (to Z.G.), and the Agence Nationale de la Recherche (ANR, ANR-08-PNANO-050 to C.G. and Z.G.). E. Mazari was a recipient of Ph. D. studentships from both the "Fondation pour la Recherche Médicale" and the "Triangle de la Physique".

Supporting Information Available: Supplementary figures and discussion. This material is available free of charge *via* the Internet at http://pubs.acs.org.

REFERENCES AND NOTES

1. Hess, H.; Clemmens, J.; Brunner, C.; Doot, R.; Luna, S.; Ernst, K. H.; Vogel, V. Molecular Self-Assembly of "Nanowires" and "Nanospools" Using Active Transport. *Nano Lett.* **2005**, *5*, 629–633.
2. Goel, A.; Vogel, V. Harnessing Biological Motors to Engineer Systems for Nanoscale Transport and Assembly. *Nat. Nanotechnol.* **2008**, *3*, 465–475.
3. Hess, H.; Bachand, G. D.; Vogel, V. Powering Nanodevices with Biomolecular Motors. *Chem.—Eur. J.* **2004**, *10*, 2110–2116.
4. Choi, D. S.; Byun, K. E.; Hong, S. Dual Transport Systems Based on Hybrid Nanostructures of Microtubules and Actin Filaments. *Small* **2011**, *7*, 1755–1760.
5. Mrksich, M.; Whitesides, G. M. Patterning Self-Assembled Monolayers Using Microcontact Printing—A New Technology for Biosensors. *Trends Biotechnol.* **1995**, *13*, 228–235.
6. Whitesides, G. M.; Ostuni, E.; Takayama, S.; Jiang, X. Y.; Ingber, D. E. Soft Lithography in Biology and Biochemistry. *Annu. Rev. Biomed. Eng.* **2001**, *3*, 335–373.
7. Blattler, T.; Huwiler, C.; Ochsner, M.; Stadler, B.; Solak, H.; Voros, J.; Grandin, H. M. Nanopatterns with Biological Functions. *J. Nanosci. Nanotechnol.* **2006**, *6*, 2237–2264.
8. Blattler, T. M.; Binkert, A.; Zimmermann, M.; Textor, M.; Voros, J.; Reimhult, E. From Particle Self-Assembly to Functionalized Sub-Micron Protein Patterns. *Nanotechnology* **2008**, *19*, 1–10.
9. Rakickas, T.; Gavutis, M.; Reichel, A.; Piehler, J.; Liedberg, B.; Valiokas, R. Protein-Protein Interactions in Reversibly Assembled Nanopatterns. *Nano Lett.* **2008**, *8*, 3369–3375.
10. Gallant, N. D.; Capadona, J. R.; Frazier, A. B.; Collard, D. M.; Garcia, A. J. Micropatterned Surfaces to Engineer Focal Adhesions for Analysis of Cell Adhesion Strengthening. *Langmuir* **2002**, *18*, 5579–5584.
11. Chen, T. H.; Guo, C. Y.; Zhao, X.; Yao, Y. C.; Bostrom, K. I.; Wong, M. N.; Tintut, Y.; Demer, L. L.; Ho, C. M.; Garfinkel, A. Patterns of Periodic Holes Created by Increased Cell Motility. *Interface Focus* **2012**, *2*, 457–464.
12. Lehnert, D.; Wehrle-Haller, B.; David, C.; Weiland, U.; Ballestrem, C.; Imhof, B. A.; Bastmeyer, M. Cell Behaviour on Micropatterned Substrata: Limits of Extracellular Matrix Geometry for Spreading and Adhesion. *J. Cell Sci.* **2004**, *117*, 41–52.
13. Fereol, S.; Fodil, P.; Barnat, M.; Georget, V.; Milbreta, U.; Nothias, F. Micropatterned ECM Substrates Reveal Complementary Contribution of Low and High Affinity Ligands to Neurite Outgrowth. *Cytoskeleton* **2011**, *68*, 373–388.
14. Lee, D. H. Fabrication of Silica Mesh Patterns *via* Self-Assembly of Block Copolymers. *Macromol. Res.* **2012**, *20*, 990–995.
15. Loverde, S. M.; Pantano, D. A.; Christian, D. A.; Mahmud, A.; Klein, M. L.; Discher, D. E. Curvature, Rigidity, and Pattern Formation in Functional Polymer Micelles and Vesicles—From Dynamic Visualization to Molecular Simulation. *Curr. Opin. Solid State Mater. Sci.* **2011**, *15*, 277–284.
16. Hamon, C.; Postic, M.; Mazari, E.; Bizien, T.; Dupuis, C.; Even-Hernandez, P.; Jimenez, A.; Courbin, L.; Gosse, C.; Artzner, F.; *et al.* Three-Dimensional Self-Assembling of Gold Nanorods with Controlled Macroscopic Shape and Local Smectic B Order. *ACS Nano* **2012**, *6*, 4137–4146.
17. Seeman, N. C. DNA in a Material World. *Nature* **2003**, *421*, 427–431.
18. Shimizu, T.; Masuda, M.; Minamikawa, H. Supramolecular Nanotube Architectures Based on Amphiphilic Molecules. *Chem. Rev.* **2005**, *105*, 1401–1443.
19. Hess, H. Self-Assembly Driven by Molecular Motors. *Soft Matter* **2006**, *2*, 669–677.
20. Reymann, A. C.; Martiel, J. L.; Cambier, T.; Blanchoin, L.; Boujemaa-Paterski, R.; Thery, M. Nucleation Geometry Governs Ordered Actin Networks Structures. *Nat. Mater.* **2010**, *9*, 827–832.
21. Sanchez, T.; Chen, D. T. N.; DeCamp, S. J.; Heymann, M.; Dogic, Z. Spontaneous Motion in Hierarchically Assembled Active Matter. *Nature* **2012**, *491*, 431–434.
22. Wong, G. C. L.; Tang, J. X.; Lin, A.; Li, Y. L.; Janmey, P. A.; Safinya, C. R. Hierarchical Self-Assembly of F-Actin and Cationic Lipid Complexes: Stacked Three-Layer Tubule Networks. *Science* **2000**, *288*, 2035–2039.
23. Boal, A. K.; Headley, T. J.; Tissot, R. G.; Bunker, B. C. Microtubule-Templated Biomimetic Mineralization of Lepidocrocite. *Adv. Funct. Mater.* **2004**, *14*, 19–24.

24. Leduc, P. R.; Robinson, D. N. Using Lessons from Cellular and Molecular Structures for Future Materials. *Adv. Mater.* **2007**, *19*, 3761–3770.
25. Henry, E.; Dif, A.; Schmutz, M.; Legoff, L.; Amblard, F.; Marchi-Artzner, V.; Artzner, F. Crystallization of Fluorescent Quantum Dots within a Three-Dimensional Bio-Organic Template of Actin Filaments and Lipid Membranes. *Nano Lett.* **2011**, *11*, 5443–5448.
26. Spoerke, E. D.; Boal, A. K.; Bachand, G. D.; Bunker, B. C. Templated Nanocrystal Assembly on Biodynamic Artificial Microtubule Asters. *ACS Nano* **2013**, *7*, 2012–2019.
27. Nedelec, F. J.; Surrey, T.; Maggs, A. C.; Leibler, S. Self-Organization of Microtubules and Motors. *Nature* **1997**, *389*, 305–308.
28. Surrey, T.; Nedelec, F.; Leibler, S.; Karsenti, E. Physical Properties Determining Self-Organization of Motors and Microtubules. *Science* **2001**, *292*, 1167–1171.
29. Bottier, C.; Fattaccioli, J.; Tarhan, M. C.; Yokokawa, R.; Morin, F. O.; Kim, B.; Collard, D.; Fujita, H. Active Transport of Oil Droplets along Oriented Microtubules by Kinesin Molecular Motors. *Lab Chip* **2009**, *9*, 1694–1700.
30. Aoyama, S.; Shimoike, M.; Hiratsuka, Y. Self-Organized Optical Device Driven by Motor Proteins. *Proc. Natl. Acad. Sci. U. S. A.* **2013**, *110*, 16408–16413.
31. Zerrouki, D.; Baudry, J.; Pine, D.; Chaikin, P.; Bibette, J. Chiral Colloidal Clusters. *Nature* **2008**, *455*, 380–382.
32. Snezhko, A. Non-Equilibrium Magnetic Colloidal Dispersions at Liquid-Air Interfaces: Dynamic Patterns, Magnetic Order and Self-Assembled Swimmers. *J. Phys.: Condens. Matter* **2011**, *23*, 1–21.
33. Erb, R. M.; Son, H. S.; Samanta, B.; Rotello, V. M.; Yellen, B. B. Magnetic Assembly of Colloidal Superstructures with Multipole Symmetry. *Nature* **2009**, *457*, 999–1002.
34. Gaetz, J.; Gueroui, Z.; Libchaber, A.; Kapoor, T. M. Examining How The Spatial Organization of Chromatin Signals Influences Metaphase Spindle Assembly. *Nat. Cell Biol.* **2006**, *8*, 924–932.
35. Brangbour, C.; du Roure, O.; Helfer, E.; Demoulin, D.; Mazurier, A.; Fermigier, M.; Carlier, M. F.; Bibette, J.; Baudry, J. Force-Velocity Measurements of a Few Growing Actin Filaments. *PLoS Biol.* **2011**, *9*, 1–7.
36. Mannix, R. J.; Kumar, S.; Cassiola, F.; Montoya-Zavala, M.; Feinstein, E.; Prentiss, M.; Ingber, D. E. Nanomagnetic Actuation of Receptor-Mediated Signal Transduction. *Nat. Nanotechnol.* **2008**, *3*, 36–40.
37. Lee, J.-H.; Kim, E. S.; Cho, M. H.; Son, M.; Yeon, S.-I.; Shin, J.-S.; Cheon, J. Artificial Control of Cell Signaling and Growth by Magnetic Nanoparticles. *Angew. Chem., Int. Ed.* **2010**, *49*, 5698–5702.
38. Steketee, M. B.; Moysidis, S. N.; Jin, X.-L.; Weinstein, J. E.; Pita-Thomas, W.; Raju, H. B.; Iqbal, S.; Goldberg, J. L. Nanoparticle-Mediated Signaling Endosome Localization Regulates Growth Cone Motility and Neurite Growth. *Proc. Natl. Acad. Sci. U. S. A.* **2011**, *108*, 19042–19047.
39. Kumar, S. Microtubule Assembly: Switched on with Magnets. *Nat. Nanotechnol.* **2013**, *8*, 162–163.
40. Hoffmann, C.; Mazari, E.; Lallet, S.; Le Borgne, R.; Marchi, V.; Gosse, C.; Gueroui, Z. Spatiotemporal Control of Microtubule Nucleation and Assembly Using Magnetic Nanoparticles. *Nat. Nanotechnol.* **2013**, *8*, 199–205.
41. Etoc, F.; Lisse, D.; Bellaiche, Y.; Piehler, J.; Coppey, M.; Dahan, M. Subcellular Control of Rac-GTPase Signalling by Magnetogenetic Manipulation Inside Living Cells. *Nat. Nanotechnol.* **2013**, *8*, 193–198.
42. Doyle, P. S.; Bibette, J.; Bancaud, A.; Viovy, J. L. Self-Assembled Magnetic Matrices for DNA Separation Chips. *Science* **2002**, *295*, 2237–2237.
43. Minc, N.; Futterer, C.; Dorfman, K. D.; Bancaud, A.; Gosse, C.; Goubault, C.; Viovy, J. L. Quantitative Microfluidic Separation of DNA in Self-Assembled Magnetic Matrixes. *Anal. Chem.* **2004**, *76*, 3770–3776.
44. Slovakova, M.; Minc, N.; Bilkova, Z.; Smadja, C.; Faigle, W.; Futterer, C.; Taverna, M.; Viovy, J. L. Use of Self Assembled Magnetic Beads for On-Chip Protein Digestion. *Lab Chip* **2005**, *5*, 935–942.
45. Saliba, A. E.; Saias, L.; Psychari, E.; Minc, N.; Simon, D.; Bidard, F. C.; Mathiot, C.; Pierga, J. Y.; Fraisier, V.; Salamero, J.; *et al.* Microfluidic Sorting and Multimodal Typing of Cancer Cells in Self-Assembled Magnetic Arrays. *Proc. Natl. Acad. Sci. U. S. A.* **2010**, *107*, 14524–14529.
46. Caudron, M.; Bunt, G.; Bastiaens, P.; Karsenti, E. Spatial Coordination of Spindle Assembly by Chromosome-Mediated Signaling Gradients. *Science* **2005**, *309*, 1373–1376.
47. Verde, F.; Berrez, J. M.; Antony, C.; Karsenti, E. Taxol-Induced Microtubule Asters in Mitotic Extracts of Xenopus Eggs—Requirement for Phosphorylated Factors and Cytoplasmic Dynein. *J. Cell Biol.* **1991**, *112*, 1177–1187.
48. Pinot, M.; Chesnel, F.; Kubiak, J. Z.; Arnal, I.; Nedelec, F. J.; Gueroui, Z. Effects of Confinement on the Self-Organization of Microtubules and Motors. *Curr. Biol.* **2009**, *19*, 954–960.
49. Liu, J.; Lawrence, E. M.; Wu, A.; Ivey, M. L.; Flores, G. A.; Javier, K.; Bibette, J.; Richard, J. Field-Induced Structures in Ferrofluid Emulsions. *Phys. Rev. Lett.* **1995**, *74*, 2828–2831.
50. Cedervall, T.; Lynch, I.; Lindman, S.; Berggard, T.; Thulin, E.; Nilsson, H.; Dawson, K. A.; Linse, S. Understanding the Nanoparticle-Protein Corona Using Methods to Quantify Exchange Rates and Affinities of Proteins for Nanoparticles. *Proc. Natl. Acad. Sci. U. S. A.* **2007**, *104*, 2050–2055.
51. Jimenez, A. M.; Roché, M.; Pinot, M.; Panizza, P.; Courbin, L.; Gueroui, Z. Towards High Throughput Production of Artificial Egg Oocytes Using Microfluidics. *Lab Chip* **2011**, *11*, 429–434.
52. Verde, F.; Berrez, J. M.; Antony, C.; Karsenti, E. Taxol-Induced Microtubule Asters in Mitotic Extracts of Xenopus Eggs: Requirement for Phosphorylated Factors and Cytoplasmic Dynein. *J. Cell Biol.* **1991**, *112*, 1177–1187.
53. Reber, S. B.; Baumgart, J.; Widlund, P. O.; Pozniakovsky, A.; Howard, J.; Hyman, A. A.; Julicher, F. XMAP215 Activity Sets Spindle Length by Controlling the Total Mass of Spindle Microtubules. *Nat. Cell Biol.* **2013**, *15*, 1116–1122.
54. Verde, F.; Dogterom, M.; Stelzer, E.; Karsenti, E.; Leibler, S. Control of Microtubule Dynamics and Length by Cyclin A- and Cyclin B-Dependent Kinases in Xenopus Egg Extracts. *J. Cell Biol.* **1992**, *118*, 1097–1108.
55. Pollard, T. D.; Cooper, J. A. Actin, a Central Player in Cell Shape and Movement. *Science* **2009**, *326*, 1208–1212.
56. Pinot, M.; Steiner, V.; Dehapiot, B.; Yoo, B. K.; Chesnel, F.; Blanchoin, L.; Kervrann, C.; Gueroui, Z. Confinement Induces Actin Flow in a Meiotic Cytoplasm. *Proc. Natl. Acad. Sci. U. S. A.* **2012**, *109*, 11705–11710.
57. Reuther, C.; Hajdo, L.; Tucker, R.; Kasprzak, A. A.; Diez, S. Biotemplated Nanopatterning of Planar Surfaces with Molecular Motors. *Nano Lett.* **2006**, *6*, 2177–2183.
58. Needleman, D. J.; Ojeda-Lopez, M. A.; Raviv, U.; Miller, H. P.; Wilson, L.; Safinya, C. R. Higher-Order Assembly of Microtubules by Counterions: From Hexagonal Bundles to Living Necklaces. *Proc. Natl. Acad. Sci. U. S. A.* **2004**, *101*, 16099–16103.
59. Huebsch, N.; Mooney, D. J. Inspiration and Application in the Evolution of Biomaterials. *Nature* **2009**, *462*, 426–432.
60. Desai, A.; Murray, A.; Mitchison, T. J.; Walczak, C. E. The Use of Xenopus Egg Extracts to Study Mitotic Spindle Assembly and Function *In Vitro*. *Methods Cell Biol.* **1999**, *61*, 385–412.
61. Kutay, U.; Izaurralde, E.; Bischoff, F. R.; Mattaj, I. W.; Gorlich, D. Dominant-Negative Mutants of Importin-Beta Block Multiple Pathways of Import and Export Through the Nuclear Pore Complex. *EMBO J.* **1997**, *16*, 1153–1163.